# Two-Dimensional Frequency-Dependent Resistance and Inductance Calculation Method for Magnetic Components with Round Conductors

Luo, Tianming ; Ghaffarian Niasar, Mohamad; Vaessen, Peter

**DOI**
10.1109/TMAG.2023.3340115

**Publication date**
2023

**Document Version**
Final published version

**Published in**
IEEE Transactions on Magnetics

# Two-Dimensional Frequency-Dependent Resistance and Inductance Calculation Method for Magnetic Components With Round Conductors

Tianming Luo[1], Mohamad Ghaffarian Niasar[1], and Peter Vaessen[1,2]

[1]Department of Electrical Sustainable Energy, Delft University of Technology, 2628 CD Delft, The Netherlands
[2]KEMA Laboratories, 6812 DE Arnhem, The Netherlands

**Magnetic components are essential parts in many power electronic applications. Their characteristics deeply impact the performances of the applications. This article proposed a 2-D calculation method for frequency-dependent winding losses and leakage inductance of magnetic components of round conductors. The method does not have any limitations on the winding arrangement and considers the impact of magnetic cores and air gaps. The method is compared with several analytical methods and the 2-D finite-element method (FEM). Measurements and 3-D FEM are also used to validate the method. The results show that the proposed method generally has more than ten times shorter computational time than 2-D FEM and comparable accuracy, which can speed up the magnetic component design.**

*Index Terms*— **Copper losses, eddy current, impedance, leakage inductance, winding.**

## NOMENCLATURE

| | |
|---|---|
| $A$ | Magnetic vector potential. |
| $B$ | Magnetic flux density. |
| $E$ | Electric field. |
| $H$ | Magnetic field. |
| $J$ | Current density. |
| $S$ | Poynting vector. |
| $S_c$ | Cross section area of conductors. |
| $I$ | Current carried by a conductor. |
| $R_{\mathrm{dc}}$ | dc resistant per unit length. |
| $Z_{\mathrm{ac}}$ | ac impedance per unit length. |
| $P$ | Power per unit length of conductors. |
| $\phi$ | Electric potential. |
| $\omega$ | Angular frequency. |
| $\sigma$ | Electric conductivity. |
| $\kappa$ | Variable, equal to $(1-j)/\delta$. |
| $\delta$ | Skin depth, equal to $(2/(\omega\sigma\mu))^{1/2}$. |
| $\mu$ | Permeability. |
| $\mu_0$ | Vaccum permeability. |
| $n$ | Order in the general solutions. |
| $\bar{A}$ | Average magnetic vector potential over the cross section of conductors. |
| $\Re$ | Real part of the value. |
| $\Im$ | Imaginary part of the value. |
| $M$ | Number of conductors. |
| $N$ | Truncated order. |
| $N_{\mathrm{r}}$ | Maximal reflection time considered in an enclosed core window. |
| $n_{\mathrm{r}}$ | Reflection time considered in an enclosed core window. |
| $I_{2N+1}$ | Identity matrix of size $2N+1$. |
| $\alpha_{pq}$ | Matrix represents the contribution from $A''_{2nq}$ and $B''_{2nq}$ to $A'_{2np}$ and $B'_{2np}$. |
| $\gamma_p$ | Vector consisted of $C_{0p}$ $A'_{2np}$ and $B'_{2np}$. |
| $\beta_{pq}$ | Vector represents the contribution from $D_{0q}$. |
| $r_0$ | Distance between the origin and reference points. |
| $j$ | Imaginary unit. |
| $J_n$ | $n$th-order Bessel function of the first kind. |
| $A'_{1n}$, $B'_{1n}$ | Coefficients before term $J_n(\kappa r)$ in the general solution of $A$ in conductors. |
| $A'_{2n}$, $B'_{2n}$ | Coefficients before term $r^n$ in the general solution of $A$ in the air. |
| $A''_{2n}$, $B''_{2n}$ | Coefficients before term $r^{-n}$ in the general solution of $A$ in the air. |
| $C_0$, $D_0$ | Coefficients in the general solution of $A$ in the air when $n=0$. |
| $A_0$ | Particular solution of $A$ in conductors and is a constant. |
| $X_p$ | $X$ coordinate of conductor $p$'s center in the global Cartesian coordinates. |
| $Y_p$ | $Y$ coordinate of conductor $p$'s center in the global Cartesian coordinates. |
| $A_{\mathrm{r}p}$ | Received part in $A$ of conductor $p$. |
| $A_{\mathrm{e}p}$ | Emitted part in $A$ of conductor $p$. |
| $k$ | Image coefficient. |
| $T$ | Intercore reflection times. |
| $\mathcal{R}$ | Reluctance in magnetic circuit. |
| $\mathcal{F}$ | Magneto-motive force (MMF) in the magnetic circuit. |

Manuscript received 22 August 2023; revised 20 October 2023; accepted 2 December 2023. Date of publication 5 December 2023; date of current version 10 January 2024. Corresponding author: T. Luo (e-mail: T.Luo-1@tudelft.nl).

Color versions of one or more figures in this article are available at https://doi.org/10.1109/TMAG.2023.3340115.

Digital Object Identifier 10.1109/TMAG.2023.3340115

## I. INTRODUCTION

ONE of the main concerns for power electronics are their efficiency and power density. Magnetic components play an important role in both aspects. Winding loss is an essential part of loss estimation during the design procedure. For a resonant converter, integrated transformers are widely adopted [1], [2], which utilize the leakage inductance as part

of converter tanks. Therefore, accurate estimation of winding loss and inductance can facilitate magnetic component design. Besides, the calculation method might repetitively run thousands of times during optimization. For this reason, the models should have both reasonable accuracy and calculation time.

Because of the fast calculation speed, analytical methods are more preferred to the finite-element method (FEM) in the first step of design. However, they are generally limited by their assumptions and can lead to low accuracy when the assumptions are not satisfied. Most analytical and empirical methods first calculate ac resistance and leakage inductance per unit length in 1-D/2-D situations and then scale it. Dowell's model [3], [4], [5], [6], [7] is a classic 1-D method to calculate ac resistance and leakage inductance. It is based on the 1-D analysis for foil windings. It can be extended to windings with different shape conductors by transforming them into foil conductors with equal dc conductance with the help of a porosity factor. When windings significantly deviate from the model's assumptions, the porosity factor cannot lead to accurate results. For ac resistance, there are also several other approaches, like Ferreira's formula [8], which is based on round conductors and several improved methods [9], [10]. Ferreira's formula ignores the interaction of eddy current between conductors and overestimates the winding loss in the compact winding. Some works, like [11], [12], and [13], use FEM to obtain factors for empirical equations. For the leakage inductance, several 2-D methods focus on low-frequency inductance [14], [15], [16], [17] and do not consider the impact of the eddy current in windings. Schlesinger and Biela [18] did a good review of these methods. Mogorovic and Dujic [19] introduced the Rogowski factor $K_w$ to Dowell's model. Besides calculating the value per unit length, Wilcox derived mutual inductance and self-inductance formulas for a coil on magnetic cores of circular cross section [20], [21].

This article is inspired by [22] and [23]. However, in these references, only energy stored or consumed in the conductor is calculated by the Poynting vector, and the existence of magnetic cores and air gaps is not considered. The method in this article considers the energy stored outside the conductor and the existence of magnetic cores and air gaps, expanding the applicable range. Because the method is based on analytical solutions it has good accuracy and shorter computation time than FEM. The proposed 2-D method's code is built and shared at [24]. The article is structured as follows. Section II introduces the construction of the 2-D method. Section III compares the results from the proposed method with results from other models, FEM simulations, and measurements for specific configurations.

## II. Proposed 2-D Method Establishment

This section introduces the basic theory of the method, including the impedance formula, the general solution of the magnetic vector potential, the multiconductor system, and how to deal with core and air gaps.

### A. Impedance Formula

The magnetic vector potential $A$ is defined in such a way that its curl is equal to the magnetic flux density $B$. It can also specify the electric field $E$, together with the electric potential $\phi$, as shown in the following equation:

$$B = \nabla \times A \text{ and } E = -\nabla\phi - j\omega A. \tag{1}$$

In the first step of the proposed method, a round conductor is analyzed in the frequency domain under 2-D quasimagneto-statics, and all quantities are complex. $A$ and $E$ only have the component perpendicular to the 2-D plane, and the coulomb gauge is adopted. Integrate the $E$ over the cross section $s$ of the conductor, and (2) is obtained based on $J = \sigma E$ and a constant $\phi$ over the cross section

$$\oiint J\, ds/\sigma S_c = -\nabla\phi - \oiint j\omega A\, ds/S_c. \tag{2}$$

The ac impedance per unit length $Z_{\text{ac}}$ in this article does not consider capacitance. If a conductor carries a certain ac current $I$ with $\omega$, the relation between $Z_{\text{ac}}$ and average magnetic vector potential $\bar{A}$ over the cross section is given in (3). The stored energy calculated by $Z_{\text{ac}}$ involves both energy inside and outside conductors. Because the analysis is done in 2-D, the value of $A$ depends on the choice of the reference point, unless the net current is zero in the case

$$Z_{\text{ac}} = R_{\text{dc}} + \frac{j\omega\bar{A}}{I}. \tag{3}$$

### B. General Solution of Magnetic Vector Potential

As (3) shown, $\bar{A}$ is required for calculating $Z_{\text{ac}}$. Therefore, this section explains how to obtain $\bar{A}$. The following partial differential equation (PDE) is obtained from Maxwell equations for 2-D quasimagneto-statics in the frequency domain:

$$\nabla^2 A - j\omega\sigma\mu A = \mu\sigma\nabla\phi. \tag{4}$$

In polar coordinates $(r, \varphi)$, as shown in Fig. 1(a), a round conductor of radius $a$ is located at the origin and is surrounded by air. There are two regions in the case. One is the conductor of conductivity $\sigma_c$, and another is the air of conductivity $\sigma = 0$. The solution for the magnetic vector potential in the conductor is the summation of the general solution of the Helmholtz equation and a particular solution, as (5). The solution for the air region is the general solution of the Laplace equation, as (6). Due to the periodical condition $A(r, \varphi) = A(r, \varphi+2\pi)$ and properties of trigonometric functions, factor $n$ can only be non-negative integers. Besides, the Bessel function of the second kind does not appear in (5) because of the limited value at the center of the conductor

$$A_{\text{c}}(r, \varphi) = A_0 + \sum_{n=0}^{+\infty} J_n(\kappa r)(A'_{1n}\cos n\varphi + B'_{1n}\sin n\varphi) \tag{5}$$

$$A_{\text{air}}(r, \varphi) = C_0 + D_0 \ln(r/r_0) + \sum_{n=1}^{+\infty} \begin{Bmatrix} r^n(A'_{2n}\cos n\varphi + B'_{2n}\sin n\varphi) \\ +r^{-n}(A''_{2n}\cos n\varphi + B''_{2n}\sin n\varphi) \end{Bmatrix} \tag{6}$$

where $A_0$ is the particular solution, $\kappa = (1-j)/\delta$, and $r_0$ is the distance to reference point. Due to Ampere's law, $D_0$ is

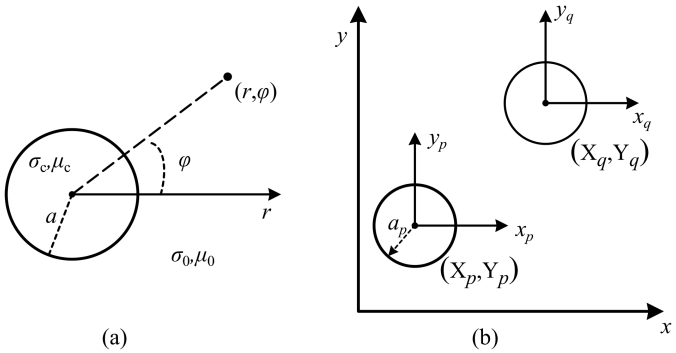


Fig. 1. Illustration of used coordinates. (a) Section II-B. (b) Section II-C.

equal to $-\mu_0 I 2\pi$. Then, the boundary condition (7) at $r = a$ needs to be fulfilled

$$\begin{aligned} \mu_c H_{r\_c}|_{r=a} &= \mu_0 H_{r\_air}|_{r=a} \\ H_{\varphi\_c}|_{r=a} &= H_{\varphi\_air}|_{r=a} \\ A_{z\_c}|_{r=a} &= A_{z\_air}|_{r=a}. \end{aligned} \tag{7}$$

In this article, the non-magnetic conductor is considered, that is, $\mu_c = \mu_0$. The relations in (8) are obtained

$$\begin{aligned} A'_{10} &= -\frac{D_0}{a\kappa J_1(\kappa a)} \\ A'_{1n} &= \frac{2na^{n-1}}{\kappa J_{n-1}(\kappa a)} A'_{2n} = \frac{2n}{a^{n+1}\kappa J_{n+1}(\kappa a)} A''_{2n}, \quad n \geq 1 \\ B'_{1n} &= \frac{2na^{n-1}}{\kappa J_{n-1}(\kappa a)} B'_{2n} = \frac{2n}{a^{n+1}\kappa J_{n+1}(\kappa a)} B''_{2n}, \quad n \geq 1 \\ A_0 &+ A'_{10} J_0(\kappa a) \\ &= C_0 + D_0 \ln(a/r_0). \end{aligned} \tag{8}$$

$\bar{A}$ is obtained by integrating the general solution (5), and the result is as shown in (9). As mentioned, $D_0$ only relates to the $I$. Lastly, $C_0$ needs to be solved

$$\bar{A} = C_0 + D_0 \ln(a/r_0) - \frac{D_0 J_2(\kappa a)}{\kappa a J_1(\kappa a)}. \tag{9}$$

Sometimes, cases with a constant external magnetic field are considered. Because the external magnetic field does not change voltage drop and total current, it does not impact impedance. The Poynting vector $S$ can be used to calculate the energy change inside conductors in this case. The power per unit length $P$ is shown in (10), where $^*$ represents conjugate

$$\begin{aligned} P = \oint S_{r=a} d\varphi = \frac{I^2}{\sigma\pi a^2} + j\omega\frac{\mu I^2}{2\pi}\frac{J_2(\kappa a)}{\kappa a J_1(\kappa a)} \\ + \frac{j\omega}{\mu}\sum_{n=1}\left(\begin{array}{c}\pi n a^{2n}\left(1+\frac{J_{n+1}(\kappa a)}{J_{n+1}(\kappa a)}\right)\left(1-\frac{J_{n+1}(\kappa^* a)}{J_{n+1}(\kappa^* a)}\right) \\ \times\left(A'_{2n}A'^*_{2n} + B'_{2n}B'^*_{2n}\right)\end{array}\right). \end{aligned} \tag{10}$$

### C. Multi-Conductor System

To solve the coefficients in (9) and (10), the idea used in [22] and [23] is adopted. The basic idea is separating (6) into two parts according to the relation between the value of $A$ and the variable $r$. One is composed of $C_0$ and $r^n$ terms. Coefficient $C_0$ is a constant, and the absolute value of $r^n$ term is positively proportional to $r$. From the physical point of view, they cannot come from the source inside the conductor, thus representing impacts from external sources. It is called the received part. The second part includes $D_0 \ln r/r_0$ term and $r^{-n}$ term, whose absolute value is negatively proportional to $r$. The first term represents the potential induced by uniformly distributed current in the conductor. The second term is caused by an eddy current in the conductor. This part's sources are inside the conductor and this part is called emitted part. Then equations can be formed by equating the received part of one conductor and the summation of emitted parts of the other conductors or sources.

In Section II-B, the general solution (6) is given in one conductor's polar coordinates. To connect the $A_{air}$ of different conductors, it is better to convert formulas into Cartesian coordinates. As shown in Fig. 1(b), there is a global Cartesian coordinates $(x, y)$ and each conductor has a Cartesian coordinates, like $(x_p, y_p)$, whose origin is the center of the conductor.

The received part $A_{rp}$ of conductor $p$ is converted to its Cartesian coordinates $(x_p, y_p)$, as shown in the following equation:

$$A_{pr} = C_{0p} + \sum_{n=1}^{+\infty}\left\{\begin{array}{l} A'_{2np}\Re((x_p + jy_p)^n) \\ + B'_{2np}\Im((x_p + jy_p)^n)\end{array}\right\}. \tag{11}$$

Then, the emitted part $A_{eq}$ of conductor $q$ is received by conductor $p$. $A_{eq}$ is converted to the coordinates $(x_p, y_p)$, like $x_p = x_q + X_q - X_p$. The results is (12), and denote $\Delta X_{pq} = X_q - X_p$ and $\Delta Y_{pq} = Y_q - Y_p$

$$\begin{aligned} A_{eq} = \frac{D_{0q}}{2}\ln\frac{(x_p - \Delta X_{pq})^2 + (y_p - \Delta Y_{pq})^2}{r_0^2} \\ + \sum_{n=1}^{+\infty}\left\{\begin{array}{l} A''_{2nq}\Re(((x_p - \Delta X_{pq}) - j(y_p - \Delta Y_{pq}))^{-n}) \\ + B''_{2nq}\Im(((x_p - \Delta X_{pq}) - j(y_p - \Delta Y_{pq}))^{-n})\end{array}\right\}. \end{aligned} \tag{12}$$

Expand both (11) and (12) using binomial expansion and Maclaurin expansion. The coefficients of the $x_p^P y_p^Q$ term for both the received part $A_{rp}$ and the emitted part $A_{eq}$ are known. The relation between factor $A'_{2nq}$ and factor $A''_{2nq}$ is known from (8). Therefore, a set of equations for a system with $M$ conductors is formed. The infinite series expansions are truncated to $N$th order to facilitate calculation. The matrix equations like (13) are formed

$$\begin{pmatrix} I_{2N+1} & \cdots & \alpha_{1M} \\ \vdots & \ddots & \vdots \\ \alpha_{M1} & \cdots & I_{2N+1} \end{pmatrix}\begin{pmatrix} \gamma_1 \\ \vdots \\ \gamma_M \end{pmatrix} = \begin{pmatrix} \sum_{q\neq 1}\beta_{1q} \\ \vdots \\ \sum_{q\neq M}\beta_{Mq} \end{pmatrix}. \tag{13}$$

The first matrix is composed of $M \times M$ sub-matrices. Each sub-matrix's size is $(2N+1) \times (2N+1)$, and all the diagonal sub-matrices are identity matrices. Matrix $\alpha_{pq}$ represents the contribution from $A''_{2nq}$ and $B''_{2nq}$ to $A'_{2np}$ and $B'_{2np}$, and $p \neq q$. Vector $\gamma_p$ is a vector representing unknown coefficients $C_{0p}$, $A'_{1np}$, and $B'_{1np}$. Vector $\beta_{pq}$ is the contribution from coefficients

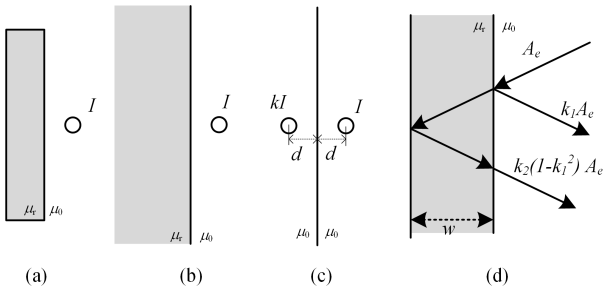


Fig. 2. (a)–(c) Application of the method of images for magnetic cores. (d) Illustration of wave reflection at magnetic cores.

$D_{0q}$. Both vectors $\gamma_p$ and $\beta_{pq}$ have $2N+1$ size. The details of the matrix are shown in the Appendix.

By solving (13), coefficients $\gamma_p$ of conductor $p$ is obtained. Then, the impedance and loss of conductor $p$ can be calculated from (3) and (10).

### D. Impact of Cores

Magnetic cores are commonly used in magnetic components, and their impacts should be considered. This section introduces how to incorporate the impact of cores into the matrix (13).

*1) Method of Images:* The method of images is a classic method to deal with specific boundary conditions [25]. As shown in Fig. 2, the boundary is replaced by an image current, whose current is $kI$, and coefficient $k$ is defined in (14). In this progress, the impacts of the finite thickness and height of the core are ignored

$$k = \frac{\mu_r - 1}{\mu_r + 1}. \tag{14}$$

The matrix (13) involving both real and image conductors can be formed. However, it dramatically increases the size of linear equations and slows down the calculation speed, which is roughly proportional to $(M(2N+1))^3$. Therefore, a reflection method is proposed based on the method of image.

*2) Reflection Method:* Compared to adding image conductors, the boundary is considered by the wave reflection idea. The emitted part $A_e$ encounters the boundary and reflects back, like Fig. 2(d). The reflection can be regarded as $A_e$ from the image conductor, which has the same $\gamma$ as the real conductor and the mirrored coordinates. In this way, the size of linear equations remains the same.

For example, assume a magnetic boundary that is perpendicular to the $x$-axis at $X_m$ in global Cartesian coordinates. When $q$ conductor produces the emitted part, the point $(x_q, y_q)$ receives a reflection, whose value is equal to the value point $(2X_m - 2X_q - x_q, y_q)$ received multiplying $k$. Then, convert to received conductor $p$'s coordinates, received value equal to the value at point $(\Delta X_{xpq} - x_p, y_p - \Delta Y_{pq})$, where $\Delta X_{xpq} = 2X_m - X_q - X_p$. The reflected emitted part from $q$ is (15). Horizontal boundaries can be solved in the same way

$$\frac{A_{xrefq}}{k} = \frac{D_{0q}}{2}\ln\left(\frac{(x_p - \Delta X_{xpq})^2 + (y_p - \Delta Y_{pq})^2}{r_0^2}\right) + \sum_{n=1}^{+\infty}\left\{\begin{matrix} A''_{2nq}\Re((-(x_p - \Delta X_{xpq}) - j(y_p - \Delta Y_{pq}))^{-n}) \\ +B''_{2nq}\Im((-(x_p - \Delta X_{xpq}) - j(y_p - \Delta Y_{pq}))^{-n})\end{matrix}\right\}. \tag{15}$$

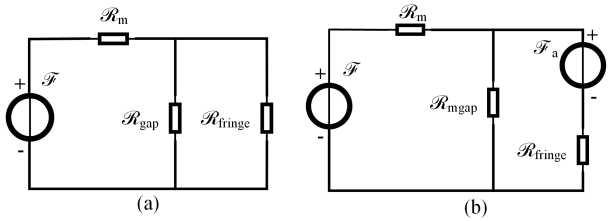


Fig. 3. (a) Magnetic circuit of a gaped core and (b) equivalent magnetic circuit with anti-MMF.

For conductors inside the core window, there are two vertical and two horizontal magnetic boundaries enclosing the conductors. Therefore, multi-time reflected parts should be taken into account, which follows the same procedure as for one boundary. After the preceding process, the impact of cores is included as

$$\begin{pmatrix} I_{2N+1} + \sum k^{n_r}\alpha_{ref11} & \cdots & \alpha_{1M} + \sum k^{n_r}\alpha_{ref1M} \\ \vdots & \ddots & \vdots \\ \alpha_{1M} + \sum k^{n_r}\alpha_{refM1} & \cdots & I_{2N+1} + \sum k^{n_r}\alpha_{refMM} \end{pmatrix} \times \begin{pmatrix} \gamma_1 \\ \vdots \\ \gamma_M \end{pmatrix} = \begin{pmatrix} \sum_{j\neq 1}\beta_{1j} + \sum k^{n_r}\beta_{ref1j} \\ \vdots \\ \sum_{j\neq M}\beta_{Mj} + \sum k^{n_r}\beta_{refMj} \end{pmatrix}. \tag{16}$$

The impact of core thickness can also be considered according to [26], as shown in Fig. 2(d). If using a perpendicular domain with a thickness $w$, the emitted part after $T$ times intercore reflection, the value is equal to the value at point $(2(X_m - X_q \pm Tw) - x_q, y_q)$ multiply $k_2^T(-k_1)^{T-1}(1-k_1^2)$. $k_1$ is the reflection coefficient at the first boundary, and $k_2$ is the coefficient at the second boundary. According to [15], the thickness is not a critical parameter in leakage inductance calculation when the thickness is above a particular value, 1 mm for $\mu_r = 2000$. Because the cores used in the next section satisfy this thickness requirement, the intercore reflection is not considered in the latter part.

### E. Impact of Air Gaps

Air gaps are widely used in inductors, and the fringe flux can cause huge proximity effect loss in the nearby conductors. Therefore, it is necessary to consider the impact of fringe flux on winding loss. In [27] and [28], the impact of the air gap is analyzed based on solving PDE and boundary conditions. However, it is complex and difficult to be incorporated into the method. Another way to consider fringe flux impact is adding an anti-MMF source and having a core without gap, used in [10], [29], and [30]. The anti-MMF source is assumed to be not influenced by the frequency and the location of conductors.

Through analyzing the magnetic circuit in Fig. 3, the relation between the MMF of all conductors $\mathcal{F}$ and the MMF of counter source $\mathcal{F}_a$ can be obtained based on equating the

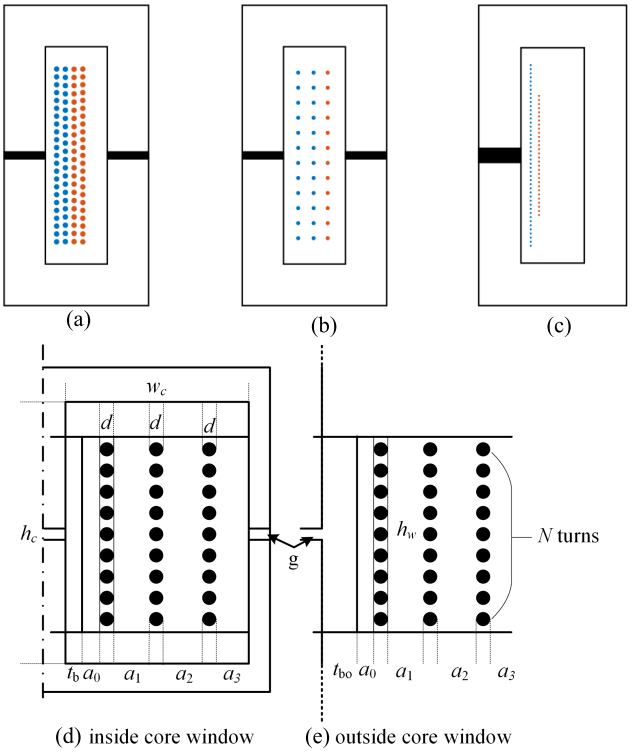


Fig. 4. Illustration of winding configurations. (a) and (b) Equal layer heights with different distances between conductors and (c) different layer heights. (d) Notation of a winding inside the core window and (e) outside the core window.

flux through $\mathcal{R}_{\text{fringe}}$ in two circuits

$$\mathcal{F}_{\text{a}} = -\frac{\mathcal{F}/\mathcal{R}_{\text{m}}}{1/\mathcal{R}_{\text{m}} + 1/\mathcal{R}_{\text{gap}} + 1/\mathcal{R}_{\text{fringe}}} \tag{17}$$

where $\mathcal{R}_{\text{m}}$ is the reluctance of core, $\mathcal{R}_{\text{gap}}$ is the reluctance of air gap, $\mathcal{R}_{\text{fringe}}$ is the reluctance of path for fringe flux, $\mathcal{R}_{\text{mgap}}$ is the reluctance of the magnetic material filling the air gap, and $\mathcal{R}_{\text{mgap}} \ll \mathcal{R}_{\text{m}}$.

This counter source can be a surface current source or a point current source. The surface current source's magnetic vector potential is represented by (18). Then, $\beta_{\text{gap}}$ representing the emitted part of the counter source is added to the matrix equations. Coefficient $C_{0\text{a}}$ is calculated based on each conductor's coefficients. If $\mathcal{F}_{\text{a}}$ is real value, the image part of $C_{0\text{a}}$ represents the losses caused by fringe flux. Assuming that the contribution from each conductor to fringe flux is proportional to its carrying current, the image part of $C_{0\text{a}}$ is correspondingly allocated to each conductor.

$$\int_g A_{\text{a}} dl = \int_g C_{0\text{a}} + D_{0\text{a}} \ln(r/r_0) dl. \tag{18}$$

## III. Simulation and Measurement

In this section, $Z_{\text{ac}}$ from the proposed method, FEM and several analytical methods are compared. For the FEM simulations, COMSOL software is used. The boundary layer feature in COMSOL is used to guarantee the accuracy of simulations. The proposed method follows the process shown in Fig. 5.

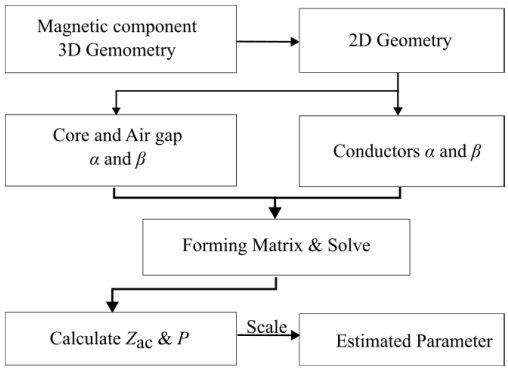


Fig. 5. Flowchart of the proposed calculation method.

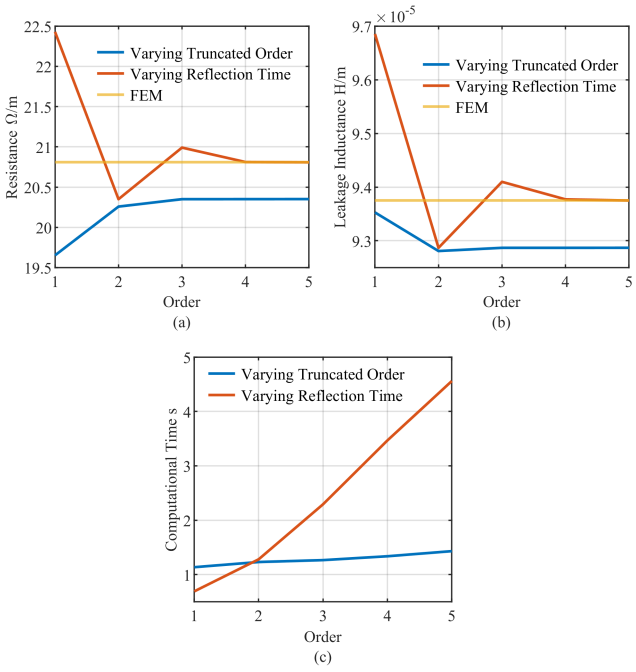


Fig. 6. (a) Resistance, (b) leakage inductance per unit length, and (c) computation time of Case 1 at 100 kHz with varying truncated order or reflection time.

Truncated order $N$ is set as 3, and the maximal considered reflection time $N_{\text{r}}$ inside the core window is set as 2. Three different configurations are computed, and transformers and inductors based on two of three windings are built and measured. In the calculation, each turn in the same winding is assigned the same current. The winding current follows the turn ratio in transformers. Results are compared with scaled estimations.

The geometries of three different configurations are shown in Fig. 4. Black parts are possible air gaps, and conductors with the same color are of the same winding. Details about the configurations are given in Table I. The semicolon in the row "Number of turns" of Table I separates the information of two windings.

### A. Proposed Method Setting Choice

In this section, the selection of $N$ and $N_{\text{r}}$ is discussed. Fig. 6(a) and (b) shows the resistance and leakage inductance

TABLE I
DETAIL INFORMATION ABOUT WINDING CONFIGURATIONS

| No. | Case (1) | Case (2) | Case (3) |
|---|---|---|---|
| Conductor radius $d$ [mm] | 0.5 | 0.4 | 0.25 |
| Conductivity $\sigma_c$ | | $5.96 \times 10^7$S/m | |
| Number of turns $N_*$ | 23,22;22,23 | 12,12;12 | 45;30 |
| Height of winding $h_w$ [mm] | 26.1 | 26.1 | 26.1;17.4 |
| Parameter $a_*$ [mm] | [0.04,0.27 ×3,3.05] | [0.63,1.45 ×2,1.98] | [0.04,0.68, 6.18] |
| Thickness of bobbin $t_b/t_{bo}$ [mm] | 1.1/1.75 | 1.1/1.75 | 1.1/1.1 |
| Air gap $g_i$ [mm] for inductor | 1 | 1 | 2 (only left leg) |
| Height of core window $h_c$ [mm] | 30.4+$g_i$ | 30.4+$g_i$ | 30.4 |
| Width of core window $w_c$ [mm] | 9 | 9 | 9 |

per unit length with varying $N$ and certain $N_r = 2$, or varying $N_r$ and certain $N = 3$. When $N$ is larger than 3, the values converge, and therefore the order is set as 3. Compared to different $N$, different $N_r$ show more influence on the result inside the core window. When $N_r$ is larger than 4, the difference is negligible. However, as (c) shows, the higher $N_r$, the longer the computation time is, therefore, $N_r$ is set to 2. From our experience, it can satisfy the requirements of general cases.

### B. AC Resistance

Winding ac resistance is one of the most important loss sources for magnetic components. In this section, the estimated resistance per unit length from 2-D FEM, the proposed method, the other two 2-D methods [10], [30], and two 1-D methods [4], [11] are compared.

First, the two windings in each case carry the current keeping total MMF zero, which represents the transformer mode. Air gaps are not applied. For cases (1) and (2), windings have equal height but do not fully fill the core window height, roughly 15% less. Therefore, 1-D methods are used. For case (3), the windings have considerable height difference, and 1-D methods are not compared.

Fig. 7 shows the results for all three cases. In (a) and (b), all methods provide less than 10% error results when $a/\delta \leq 1$ compared to 2-D FEM. The three 2-D methods have less error than the two 1-D methods. However, Mühlethaler's approach has significant errors when the frequency is high. For case (2), which has a larger distance between turns, the three 2-D approaches still have more accurate results. Dowell's method overestimates significantly at high frequency, and another 1-D method underestimates less than 10%. In case (3), the proposed method shows a more stable result than the other 2-D methods. Based on the results for the cases without air gap, the three 2-D methods show similar results when $a/\delta \leq 1$. The proposed method gives less than 3% error in all situations and is more stable than the other two 2-D methods.

Then, the two windings in each case carry the same current, that is, connect in series, and air gaps are applied, which

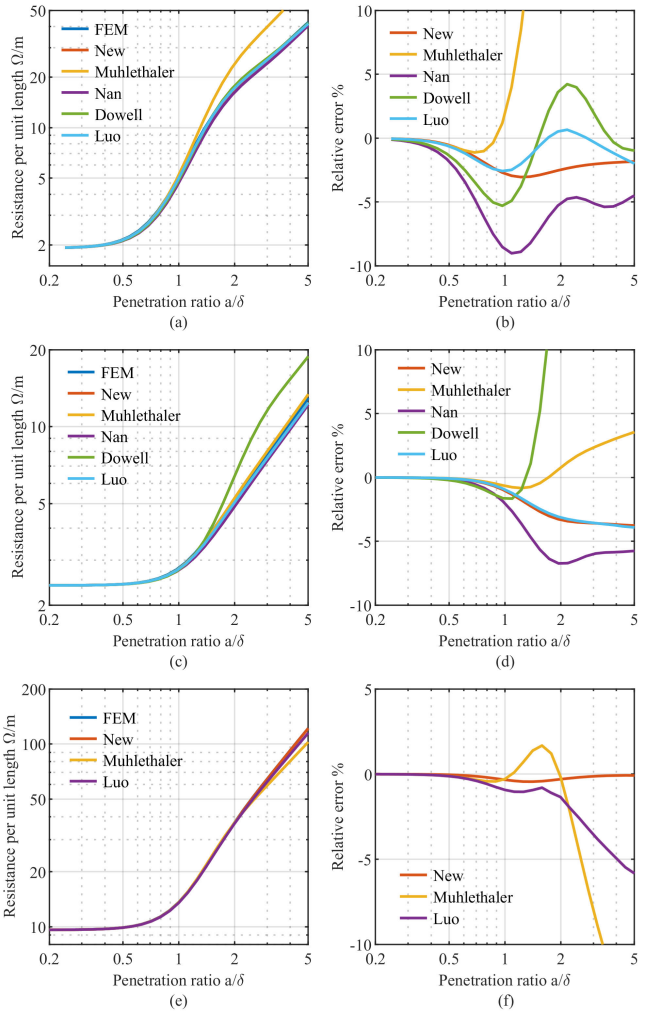


Fig. 7. Resistances per unit length and relative error compared to 2-D FEM in the transformer mode without air gap. (a) and (b) Case (1). (c) and (d) Case (2). (e) and (f) Case (3).

represents the inductor mode. Only three 2-D methods are compared with 2-D FEM because 1-D methods cannot deal with air gaps. Due to the possible considerable difference between the situation inside and outside the core window, the ac resistance is calculated under both situations. It needs to be mentioned that to keep the sample level fringe flux, the air gap outside the core window FEM is replaced by a magnetic core with a surface current density. In cases (1) and (2), there are two gaps on different core legs. Therefore, the ac resistance per unit length is estimated in two situations, that is, winding inside and outside core windows. Fig. 8 shows the results for all cases in inductor mode. All methods provide less than 10% error results when $a/\delta \leq 1$. The proposed method obviously shows more stable and accurate results compared to the other two 2-D methods, and the relative differences compared to FEM are quite small, less than 1%.

### C. Leakage Inductance

The leakage inductance per unit length is calculated for all cases in transformer mode. The FEM, proposed method, two

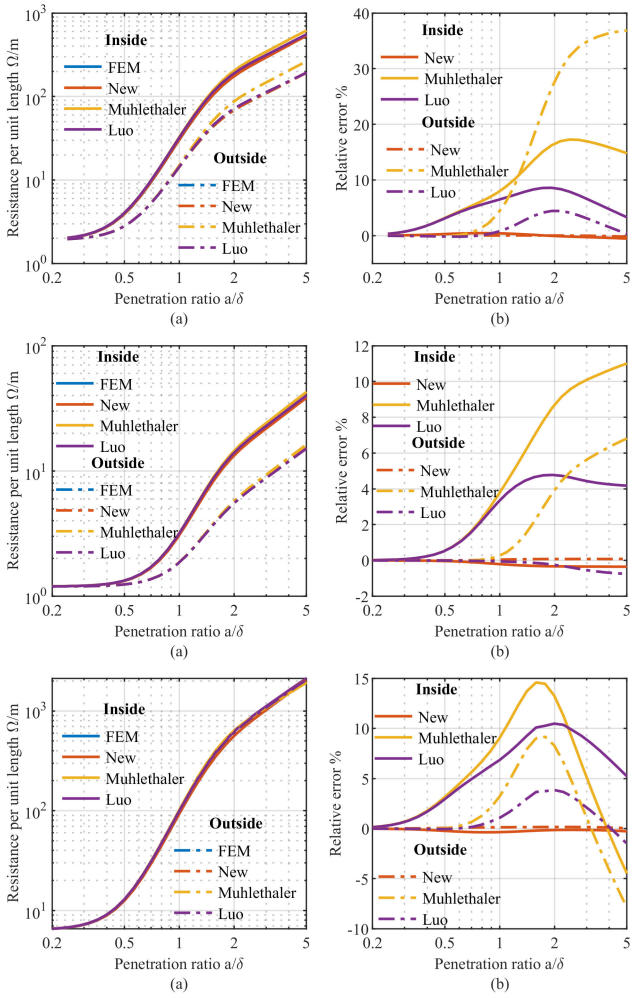


Fig. 8. Resistances per unit length and relative error compared to 2-D FEM in the inductor mode with air gap. (a) and (b) Case (1). (c) and (d) Case (2). (e) and (f) Case (3).

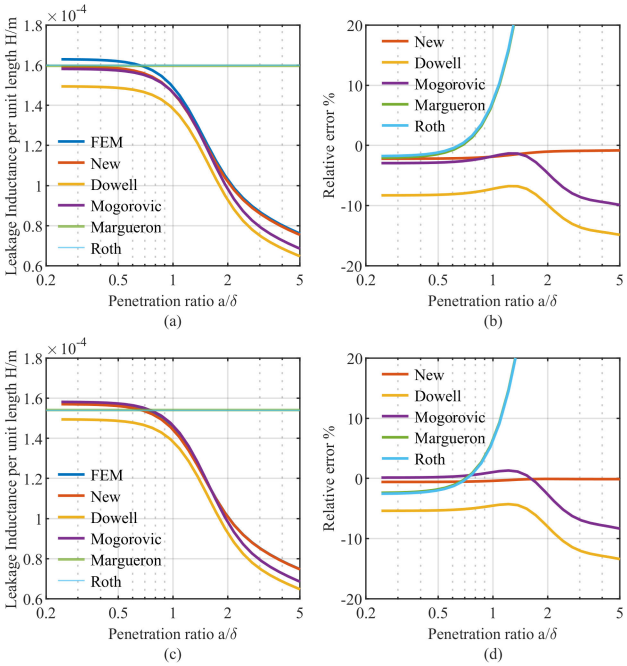


Fig. 9. Leakage inductance per unit length and relative error compared to 2-D FEM of the case (1). (a) and (b) Inside the core window. (c) and (d) Outside the core window.

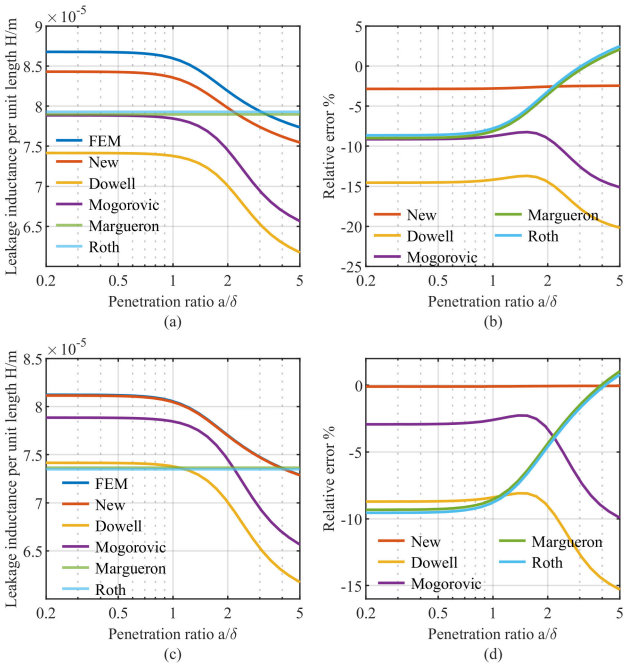


Fig. 10. Leakage inductance per unit length and relative error compared to 2-D FEM of the case (2). (a) and (b) Inside the core window. (c) and (d) Outside the core window.

frequency-related methods [3], [19] and two static methods [15], [17] are used. Besides, considering the possible difference between the inside and outside core window [18], the leakage inductance per unit length is also calculated for both situations.

Fig. 9 shows the results of case (1). First, the leakage inductance for low frequencies has close results except for Dowell's model. It implies that the Rogowski factor $K_w$ can improve the accuracy of Dowell's model when the windings have equal heights and compact alignments of conductors. Two static methods deviate from FEM results for increasing frequencies. The proposed method has less than 3% error in the whole frequency range and is closer than the other two methods considering eddy current.

Fig. 10 shows the results of case (2). For the low-frequency range, the error from other methods in case (2) is much larger than in case (1) because of the large distance between turns. Two static methods could reduce the error by considering each turn as a winding. The proposed method still has less than a 3% error and follows the FEM curve.

Fig. 11 shows the results of case (3). In the low-frequency range, the static methods have roughly 3% error because turns align compactly. However, Dowell's model and Mogorovic's improvement cannot handle windings with different heights because both of them assumed equal height windings. The

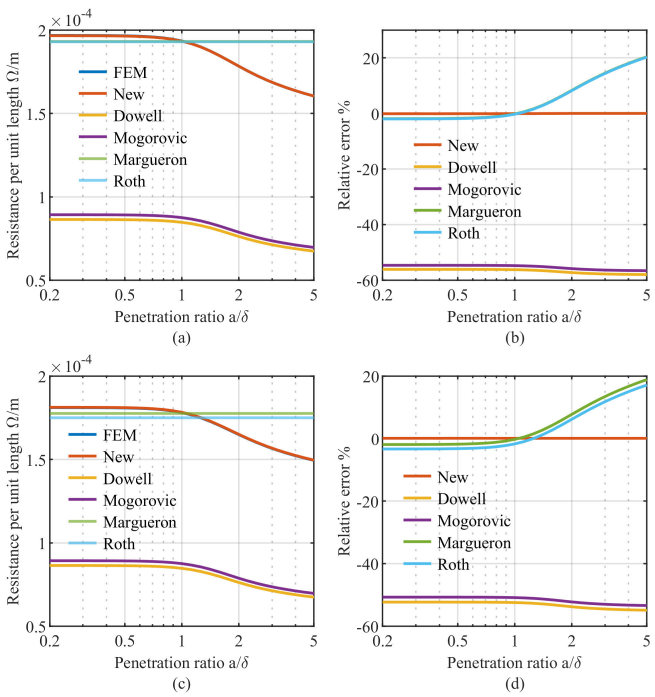


Fig. 11. Leakage inductance per unit length and relative error compared to 2-D FEM of the case (3). (a) and (b) Inside the core window. (c) and (d) Outside the core window.

TABLE II
COMPUTATION TIME OF THREE CASES WITH 41 FREQUENCY POINTS

| Item | Case1 | Case2 | Case3 |
|---|---|---|---|
| 2D FEM inside core window | 135s | 64s | 73s |
| 2D FEM outside core window | 123s | 63s | 75s |
| Proposed method inside core window | 2.09s | 0.35s | 1.47s |
| Proposed method outside core window | 1.12s | 0.16s | 0.78s |

proposed method has a similar performance as in the previous two cases.

Except for the accuracy, the computation time is another important feature. Table II compares computation time for three cases with 41 frequency points from FEM and the proposed method. For all situations, the proposed method is more than 50 times faster than FEM.

### D. Measurement and 3-D FEM

In the preceding part, comparisons are based on 2-D FEM. To further validate the method in real situations, 3-D FEM and measurement are done.

Three-dimensional FEMs for case (1) and case (2) in both transformer and inductor modes were simulated. To guarantee the accuracy of computation, the boundary layer mesh is used, and the smallest size of an element is smaller than one-third of skin depth based on analysis in [31]. Two corresponding samples were built, as shown in Fig. 12, and their details are listed in Table III. Using different connections, two samples can become transformers or inductors. The measurements are done by the impedance analyzer Agilent 4294A.

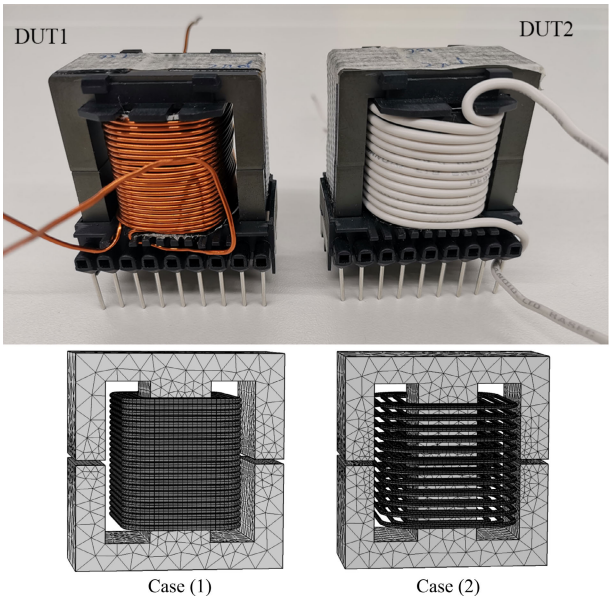


Fig. 12. Picture and 3-D FEM mesh of test samples, right is the case (1) and left is the case (2).

TABLE III
BASIC INFORMATION FOR SAMPLES

| Sample | Case (1) | Case (2) |
|---|---|---|
| Core size | EE42/21/20 | |
| Core material | N87 | |
| Effective magnetic length $l_e$ [mm] | 97 | |
| Effective magnetic cross-section $S_c[mm^2]$ | 234 | |
| Mean turn legnth $l_m$ [mm] | 90.76 | 95.97 |
| Partial length inside core window $l_{in}$ [mm] | 40 | 40 |
| Partial length outside core window $l_{out}$ [mm] | 50.76 | 55.97 |

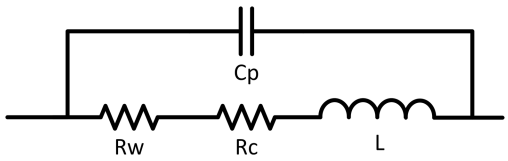


Fig. 13. Equivalent circuit of inductors.

The short circuit method was used to measure transformers' leakage inductance and winding losses. The core losses are assumed negligible. The resonant frequency is in the region $a/\delta > 15$, far from the interested region $a/\delta < 5$, and the measured ac resistance does not need correction. However, core loss is considerable for inductors. Due to the potential error from inaccurate complex permeability, an auxiliary transformer based on [32] is used to estimate core loss. Besides, the impact of parasitic capacitance $C_p$ is compensated based on an equivalent circuit of inductors, as shown in Fig. 13. After compensation, the summation of winding resistance $R_w$ and core resistance $R_c$ is obtained.

Estimated 2-D values need scaling before comparing with 3-D FEM and measurement. Generally, the value is scaled by

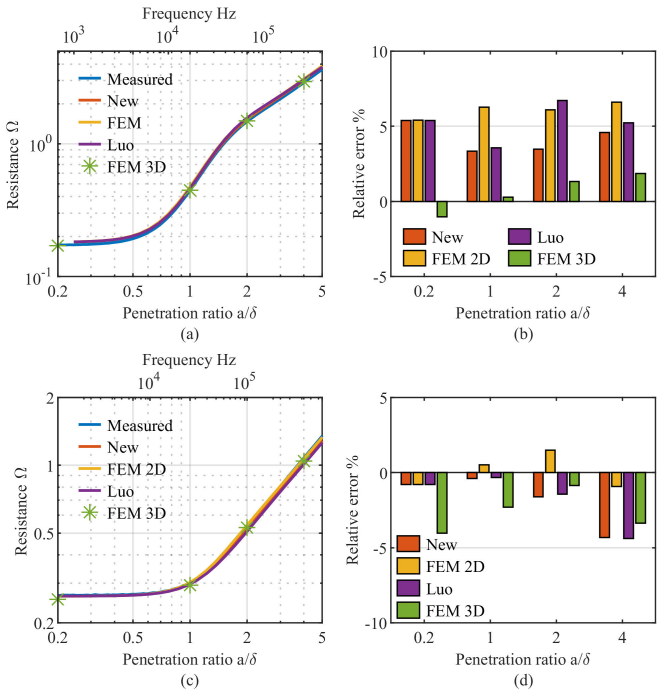


Fig. 14. Resistance and relative error of estimations in transformer mode. (a) and (b) Case (1). (c) and (d) Case (2).

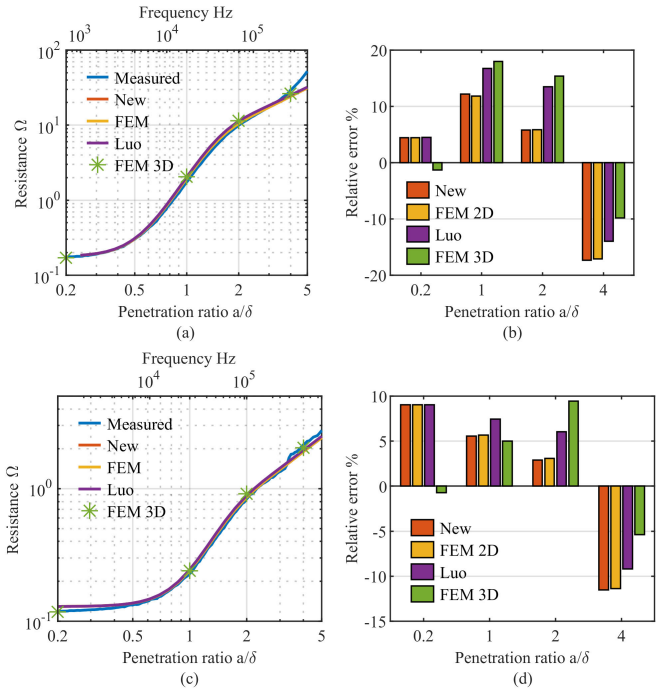


Fig. 15. Resistance and relative error of estimations in inductor mode. (a) and (b) Case (1). (c) and (d) Case (2).

the mean turn length (MTL) $l_m$. However, the values inside and outside the core window can be significantly different. Then the scaling can use a double 2-D method [10], [18], [33]. Based on 2-D FEM results, transformers' resistances use normal MTL, leakage inductances and inductors' resistances use the double 2-D method. The relevant parameters for scaling are listed in Table III.

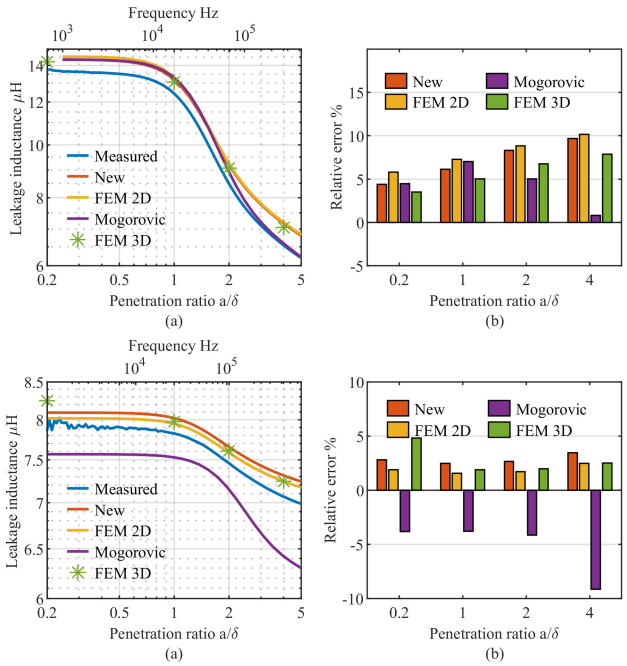


Fig. 16. Leakage inductance and relative error of estimations in inductor mode. (a) and (b) Case (1). (c) and (d) Case (2).

Fig. 14 shows the resistance of transformers. In both cases, the scaled results are close to the results from measurement and 3-D FEM. The error stays below 10% for the whole frequency range. Compared to another 2-D approach, the proposed method does not perform much better. However, it can estimate the leakage inductance at the same time.

Fig. 15 shows the resistance for samples in the inductor mode. Compared to the transformer mode, scaled resistances and 3-D FEM have obviously larger differences from measurements. In both cases, 3-D FEM results match 2-D estimations better than measurement. The maximal error is close to 20% in case (1) and approximates 10% in case (2). Several aspects contribute to the difference between measurement and estimation. The first one is the resonant compensation. When the testing frequency is near the resonant frequency, the impedance is very sensitive to the frequency. For this case, the accuracy of the circuit and resonant frequency are important. For case (1), the measured resonant frequency is at 493.8 kHz and the point $a/\delta = 4$ is at 270 kHz, which is close to the resonant frequency. The second aspect is the inequality between the 3-D and double 2-D methods. The difference between the 3-D FEM and scaled results implies that some error comes from this inequality. Next is the core loss prediction. When the core losses are comparable to winding losses, the error in the core loss estimation can lead to considerable differences in winding resistance. Besides, factors like imperfect geometric parameters and impedance phase measurement errors can also lead to winding resistance errors.

Fig. 16 shows the leakage inductance of transformers. Based on the performance in 2-D comparison, estimation from Morgorovic's method is compared with the proposed method. In general, the relative differences between measurements

and estimations stay below 10% for both cases. The scaled estimations from 2-D FEM are more close to the results from 3-D FEM than to the measurements.

## IV. Conclusion

This article proposes a 2-D method for winding losses and leakage inductance based on magnetic vector potential. The method considers the possible existence of cores and air gaps and does not have limitations on winding arrangements. For 2-D models, the proposed method has less than 5% error for all settings compared to 2-D FEM and ten times faster computational time. Besides, it is more stable than other estimation methods for various winding arrangements. The scaled estimated values show good accuracy compared to 3-D FEM and a bit higher error compared to actual measurements. The proposed 2-D method can speed up the magnetic component design.

## Appendix
## Detail of Matrix

In this Appendix, the sub-matrices $\gamma_p$, $\beta_{pq}$, and $\alpha_{pq}$ used in the model construction are given. In each matrix, symbol $n$ varies with column and $m$ varies with row from 1 to $N$

$$\gamma_p = \begin{pmatrix} C_{0p} \\ N\begin{cases} A'_{2np} \\ \vdots \end{cases} \\ N\begin{cases} B'_{2np} \\ \vdots \end{cases} \end{pmatrix} \tag{19}$$

$$\beta_{pq} = \begin{pmatrix} D_q/2 \ln \frac{\Delta X_{pq}^2 + \Delta Y_{pq}^2}{r_0^2} \\ -\frac{D_q}{m} \Re((\Delta X_{pq} - j\Delta Y_{pq})^{-m}) \\ \vdots \quad m = 1, 2, \ldots N \\ -\frac{D_q}{m} \Im((\Delta X_{pq} - j\Delta Y_{pq})^{-m}) \\ \vdots \quad m = 1, 2, \ldots, N \end{pmatrix} \tag{20}$$

$$\alpha_{pq} = \begin{pmatrix} 0 & \Re_{pqn0_{(1\times N)}} & \Im_{pqn0_{(1\times N)}} \\ 0_{(N\times 1)} & \Re_{pqnm_{(N\times N)}} & \Im_{pqnm_{(N\times N)}} \\ 0_{(N\times 1)} & -1^{n_r} \Im_{pqnm_{(N\times N)}} & -1^{n_r+1} \Re_{pqnm_{(N\times N)}} \end{pmatrix} \tag{21}$$

$$\begin{aligned} \Re_{pqnm} &= \lambda_{qnm} \Re\left(\frac{-1^n}{(\Delta X_{pq} - j\Delta Y_{pq})^{n+m}}\right) \\ \Im_{pqnm} &= \lambda_{qnm} \Im\left(\frac{-1^n}{(\Delta X_{pq} - j\Delta Y_{pq})^{n+m}}\right) \\ \lambda_{qnm} &= -\frac{a_q^{2n} J_{n+1}(\kappa a_q)}{J_{n-1}(\kappa a_q)} \frac{(n+m-1)!}{(n-1)!m!}. \end{aligned} \tag{22}$$

When constructing the matrix from reflection, $\Re_{pqnm}$ and $\Im_{pqnm}$ in (22) have different forms. Besides, $n_r$ is the times of reflection the submatrix presents. For the case involving odd $x$ reflection and even $y$ reflection, that is, reflected at vertical boundary for odd times and horizontal boundary for even times, parameters $\Re_{pqnm}$ and $\Im_{pqnm}$ should be (23), and $\Delta X_{xpq} = 2X_m - X_q - X_p$.

$$\begin{aligned} \Re_{pqnm} &= \lambda_{qnm} \Re\left(\frac{1}{(\Delta X_{xpq} + j\Delta Y_{pq})^{n+m}}\right) \\ \Im_{pqnm} &= \lambda_{qnm} \Im\left(\frac{1}{(\Delta X_{xpq} + j\Delta Y_{pq})^{n+m}}\right). \end{aligned} \tag{23}$$

For the case involving even $x$ reflection and odd $y$ reflection, two parameters should be (24), and $\Delta Y_{ypq} = 2Y_m - Y_q - Y_p$.

$$\begin{aligned} \Re_{pqnm} &= \lambda_{qnm} \Re\left(\frac{-1^n}{(\Delta X_{pq} + j\Delta Y_{ypq})^{n+m}}\right) \\ \Im_{pqnm} &= \lambda_{qnm} \Im\left(\frac{-1^n}{(\Delta X_{pq} + j\Delta Y_{ypq})^{n+m}}\right). \end{aligned} \tag{24}$$

For the case involving odd $x$ reflection and odd $y$ reflection, two parameters should be in the following equation:

$$\begin{aligned} \Re_{pqnm} &= \lambda_{qnm} \Re\left(\frac{1}{(\Delta X_{pqx} - j\Delta Y_{ypq})^{n+m}}\right) \\ \Im_{pqnm} &= \lambda_{qnm} \Im\left(\frac{1}{(\Delta X_{pqx} - j\Delta Y_{ypq})^{n+m}}\right). \end{aligned} \tag{25}$$

## Acknowledgment

The work was supported by the China Scholarship Council under Grant 202007720032.

## References

[1] H. Choi, "Analysis and design of LLC resonant converter with integrated transformer," in *Proc. IEEE Appl. Power Electron. Conf. Expo. (APEC)*, Feb. 2007, pp. 1630–1635.

[2] R.-L. Lin and L.-H. Huang, "Efficiency improvement on LLC resonant converter using integrated LCLC resonant transformer," *IEEE Trans. Ind. Appl.*, vol. 54, no. 2, pp. 1756–1764, Mar. 2018.

[3] Z. Ouyang, J. Zhang, and W. G. Hurley, "Calculation of leakage inductance for high-frequency transformers," *IEEE Trans. Power Electron.*, vol. 30, no. 10, pp. 5769–5775, Oct. 2015. [Online]. Available: http://ieeexplore.ieee.org. http://ieeexplore.ieee.org/document/6990634/

[4] P. L. Dowell, "Effects of eddy currents in transformer windings," *Proc. Inst. Electr. Eng.*, vol. 113, no. 8, p. 1387, 1966. [Online]. Available: https://digital-library.theiet.org/content/journals/10.1049/piee.1966.0236

[5] M. A. Bahmani and T. Thiringer, "Accurate evaluation of leakage inductance in high-frequency transformers using an improved frequency-dependent expression," *IEEE Trans. Power Electron.*, vol. 30, no. 10, pp. 5738–5745, Oct. 2015. [Online]. Available: https://ieeexplore.ieee.org/document/6957550/

[6] R. P. Wojda and M. K. Kazimierczuk, "Winding resistance of litz-wire and multi-strand inductors," *IET Power Electron.*, vol. 5, no. 2, p. 257, 2012. [Online]. Available: https://digital-library.theiet.org/content/journals/10.1049/iet-pel.2010.0359

[7] D. Whitman and M. K. Kazimierczuk, "An analytical correction to Dowell's equation for inductor and transformer winding losses using cylindrical coordinates," *IEEE Trans. Power Electron.*, vol. 34, no. 11, pp. 10425–10432, Nov. 2019. [Online]. Available: https://ieeexplore.ieee.org/document/8665954/

[8] J. A. Ferreira, "Improved analytical modeling of conductive losses in magnetic components," *IEEE Trans. Power Electron.*, vol. 9, no. 1, pp. 127–131, Jan. 1994. [Online]. Available: https://ieeexplore.ieee.org/document/285503/

[9] M. Bartoli, N. Noferi, A. Reatti, and M. K. Kazimierczuk, "Modelling winding losses in high-frequency power inductors," *J. Circuits, Syst. Comput.*, vol. 5, no. 4, pp. 607–626, Dec. 1995. [Online]. Available: https://www.worldscientific.com/doi/abs/10.1142/S0218126695000370

[10] J. Mühlethaler, J. W. Kolar, and A. Ecklebe, "Loss modeling of inductive components employed in power electronic systems," in *Proc. 8th Int. Conf. Power Electron.-ECCE Asia, Green World with Power Electron. (ICPE-ECCE Asia)*, May 2011, pp. 945–952. [Online]. Available: http://ieeexplore.ieee.org/document/5944652/

[11] X. Nan and C. R. Sullivan, "Simplified high-accuracy calculation of eddy-current loss in round-wire windings," in *Proc. IEEE 35th Annu. Power Electron. Spec. Conf.*, Jun. 2004, pp. 873–879. [Online]. Available: http://ieeexplore.ieee.org/document/1355533/

[12] M. A. Bahmani, T. Thiringer, and H. Ortega, "An accurate pseudoempirical model of winding loss calculation in HF foil and round conductors in switchmode magnetics," *IEEE Trans. Power Electron.*, vol. 29, no. 8, pp. 4231–4246, Aug. 2014. [Online]. Available: http://ieeexplore.ieee.org/document/6675076/

[13] G. S. Dimitrakakis, E. C. Tatakis, and E. J. Rikos, "A semiempirical model to determine HF copper losses in magnetic components with nonlayered coils," *IEEE Trans. Power Electron.*, vol. 23, no. 6, pp. 2719–2728, Nov. 2008.

[14] X. Margueron, J.-P. Keradec, and D. Magot, "Analytical calculation of static leakage inductances of HF transformers using PEEC formulas," *IEEE Trans. Ind. Appl.*, vol. 43, no. 4, pp. 884–892, Jul. 2007.

[15] X. Margueron, A. Besri, P.-O. Jeannin, J.-P. Keradec, and G. Parent, "Complete analytical calculation of static leakage parameters: A step toward HF transformer optimization," *IEEE Trans. Ind. Appl.*, vol. 46, no. 3, pp. 1055–1063, May 2010. [Online]. Available: http://ieeexplore.ieee.org/document/5438749/

[16] S. Kulkarni and S. Khaparde, *Transformer Engineering*. Boca Raton, FL, USA: CRC Press, May 2004. [Online]. Available: https://www.taylorfrancis.com/books/9780824757281

[17] A. Boyajian, "Leakage reactance of irregular distributions of transformer windings by the method of double Fourier series [includes discussion]," *Trans. Amer. Inst. Electr. Eng. III, Power App. Syst.*, vol. 73, no. 2, pp. 1078–1086, Jan. 1954. [Online]. Available: http://ieeexplore.ieee.org/document/4498933/

[18] R. Schlesinger and J. Biela, "Comparison of analytical models of transformer leakage inductance: Accuracy versus computational effort," *IEEE Trans. Power Electron.*, vol. 36, no. 1, pp. 146–156, Jan. 2021. [Online]. Available: https://ieeexplore.ieee.org/document/9112706/

[19] M. Mogorovic and D. Dujic, "Medium frequency transformer leakage inductance modeling and experimental verification," in *Proc. IEEE Energy Convers. Congr. Expo. (ECCE)*, Oct. 2017, pp. 419–424. [Online]. Available: http://ieeexplore.ieee.org/document/8095813/

[20] D. J. Wilcox, M. Conlon, and W. G. Hurley, "Calculation of self and mutual impedances for coils on ferromagnetic cores," *IEE Proc. A Phys. Sci., Meas. Instrum., Manage. Educ., Rev.*, vol. 135, no. 7, p. 470, 1988. [Online]. Available: https://digital-library.theiet.org/content/journals/10.1049/ip-a-1.1988.0074

[21] W. G. Hurley and D. J. Wilcox, "Calculation of leakage inductance in transformer windings," *IEEE Trans. Power Electron.*, vol. 9, no. 1, pp. 121–126, Jan. 1994. [Online]. Available: https://ieeexplore.ieee.org/document/285502/

[22] S. Butterworth, "III. Eddy-current losses in cylindrical conductors, with special applications to the alternating current resistances of short coils," *Phil. Trans. Roy. Soc. London A, Containing Papers Math. Phys. Character*, vol. 222, nos. 594–604, pp. 57–100, Jan. 1922. [Online]. Available: https://royalsocietypublishing.org/doi/10.1098/rsta.1922.0003

[23] T. Delaforge and H. Chazal, "Formal solution based on the magnetic potential for round conductive area," *IEEE Trans. Magn.*, vol. 54, no. 12, pp. 1–8, Dec. 2018. [Online]. Available: https://ieeexplore.ieee.org/document/8490113/

[24] T. Luo. (2023). *MultiCon2D_L*. [Online]. Available: https://github.com/TMLuo/MultiCon2D_L

[25] P. Hammond, "Electric and magnetic images," *Proc. IEE C, Monographs*, vol. 107, no. 12, p. 306, 1960. [Online]. Available: https://digital-library.theiet.org/content/journals/10.1049/pi-c.1960.0047

[26] P. Silvester, "TEM wave properties of microstrip transmission lines," *Proc. Inst. Electr. Engineers*, vol. 115, no. 1, p. 43, 1968. [Online]. Available: https://digital-library.theiet.org/content/journals/10.1049/piee.1968.0008

[27] M. Albach and H. Rossmanith, "The influence of air gap size and winding position on the proximity losses in high frequency transformers," in *Proc. IEEE 32nd Annu. Power Electron. Spec. Conf.*, vol. 3, Jun. 2001, pp. 1485–1490. [Online]. Available: http://ieeexplore.ieee.org/document/954329/

[28] P. Wallmeier, "Improved analytical modeling of conductive losses in gapped high-frequency inductors," *IEEE Trans. Ind. Appl.*, vol. 37, no. 4, pp. 1045–1054, Jul. 2001.

[29] A. Van den Bossche and V. C. Valchev, *Inductors and Transformers for Power Electronics*. Boca Raton, FL, USA: CRC Press, 2005.

[30] T. Luo, M. G. Niasar, and P. Vaessen, "2-D winding losses calculation for round conductor coil," *IEEE Trans. Power Electron.*, vol. 38, no. 4, pp. 5107–5117, Apr. 2023.

[31] L. Taylor, X. Margueron, Y. Le Menach, and P. Le Moigne, "Numerical modelling of PCB planar inductors: Impact of 3D modelling on high-frequency copper loss evaluation," *IET Power Electron.*, vol. 10, no. 14, pp. 1966–1974, Nov. 2017. [Online]. Available: https://onlinelibrary.wiley.com/doi/10.1049/iet-pel.2017.0086

[32] K. Niyomsatian, J. J. C. Gyselinck, and R. V. Sabariego, "Experimental extraction of winding resistance in litz-wire transformers—Influence of winding mutual resistance," *IEEE Trans. Power Electron.*, vol. 34, no. 7, pp. 6736–6746, Jul. 2019.

[33] R. Prieto, J. Cobos, O. Garcia, P. Alou, and J. Uceda, "Study of 3-D magnetic components by means of 'double 2-D' methodology," *IEEE Trans. Ind. Electron.*, vol. 50, no. 1, pp. 183–192, Feb. 2003. [Online]. Available: http://ieeexplore.ieee.org/document/1174074/